

Function of Aramid Separator (Pervio) in Lithium-ion Battery



Sumitomo Chemical Co., Ltd.
Energy & Functional Materials Research Laboratory
Ichiro ARISE*
Tomoaki OZEKI
Kyoto University
Department of Energy and Hydrocarbon Chemistry
Yuto MIYAHARA
Kohei MIYAZAKI
Takeshi ABE

In recent years, many efforts have been discussed and implemented around the world to achieve the Sustainable Development Goals (SDGs). The widespread use of fossil fuel-free electric vehicles (EVs) is essential for solving energy and climate change issues, which is one of the 17 SDGs. Our product, named Pervio, is Aramid Coated Separator (ACS) for lithium-ion batteries (LIBs) that is used in EV batteries, and there is a possibility that it may improve safety. In this paper, we report on the functions and features of our ACS in LIBs.

This paper is translated from R&D Report, "SUMITOMO KAGAKU", vol. 2022.

Introduction

In recent years, many efforts have been discussed and implemented around the world to achieve the Sustainable Development Goals (SDGs). The widespread use of fossil fuel-free electric vehicles (EVs), which do not emit CO₂ when driven, is essential for solving energy and climate change issues, which is one of the 17 SDGs, and the demand for EV batteries is increasing.

Many of today's EVs use lithium-ion rechargeable batteries as their main power source, and achieving both high output and high energy density over a wide temperature range is a key challenge for these batteries¹⁾. However, batteries with high energy density have a high risk of ignition in the event of an internal short circuit or other malfunction.

There is a trade-off between high energy density and safety, and one of the most important battery components for ensuring safety is the separator. The separator is placed between the cathode and anode and has the function of insulating the cathode and anode. It also has the function of blocking the flow of lithium ions when excessive heat is generated, as the heat will melt the pores of the separator, causing it to have no pores, thus providing lithium ions with a blocking function.²⁾⁻⁵⁾.

The separator is made of a porous polyolefin base film, and to further improve thermal resistance, a ceramic is coated on top of this base film. These are called ceramic-coated separators.

In recent years, as the required energy density has increased, designs that reduce the capacitance ratio of the cathode/anode (AC ratio) and the use of lithium metal anodes have been studied, but these cause lithium dendritic compounds to deposit on the negative electrode. Lithium metal anodes have long been known to form dendrite and have only been used in lithium-air batteries and primary lithium batteries.

Our product, named Pervio, is Aramid Coated Separator (ACS) for lithium-ion batteries. It contains aramid resin in the coating layer, and its dense pore structure has been found to have the potential to control lithium dendrite deposition and improve safety.

In this paper, we report on the features of our ACS and its functions in lithium-ion secondary batteries.

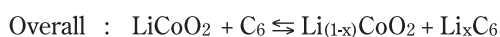
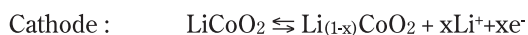
Lithium-ion secondary battery

1. Principle and configuration of lithium-ion secondary batteries

Normally, a lithium-ion secondary battery has a separator between its cathode and anode, and is filled with electrolyte. Typical materials for lithium-ion secondary batteries include metal oxides composed of lithium

* Current department: IT-Related Chemicals Research Laboratory

combined with nickel, cobalt, manganese, and aluminum for the cathode, graphite or silicon for the anode, a porous polyolefin membrane for the separator, and organic electrolyte dissolved with lithium salt for the electrolyte. **Fig. 1** shows the configuration of a lithium-ion secondary battery including these components. The reactions of the cathode and anode are shown below:



As shown schematically in **Fig. 1**, in a typical lithium-ion secondary battery (cathode: LCO (Lithium Cobalt Oxide), anode: graphite), both the cathode and anode have a layered structure. In its initial state, lithium is filled between the layers of the cathode. During charging, the lithium in the cathode is extracted and inserted between the layers of the anode.

As the above overall reaction indicates, lithium ions are not normally directly reduced. For this reason, lithi-

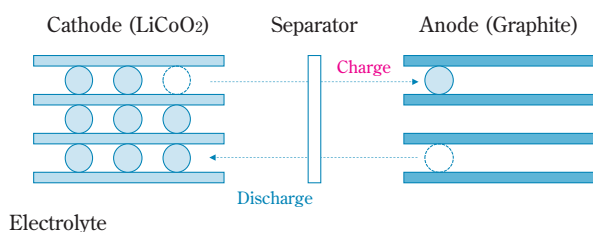


Fig. 1 Structure and principal of lithium-ion batteries

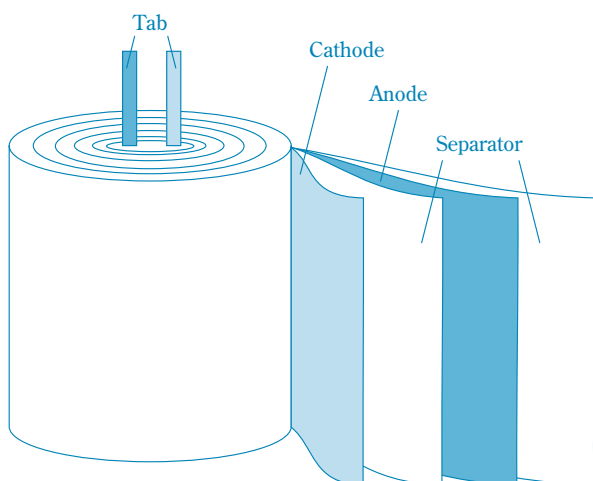


Fig. 2 Jelly roll configuration of commercial batteries

um-ion secondary batteries are called rocking-chair batteries, in which lithium ions are repeatedly transported between the cathode and anode.

Battery bodies (battery cells) are usually configured to have a separator between the cathode and anode. The arrangement of these components is often made by stacking each part or by winding them as a single unit, as illustrated in **Fig. 2** (this wound body is generally referred to as a jelly roll). In commercial lithium-ion batteries, the electrode thickness is about 10 to 100 μm per side, while the separator thickness is often very thin (5 to 30 μm), so the separator must have high mechanical strength. The well-known batteries are the jelly-roll type, or the stacked type. Their electrode is inserted into a can or aluminum laminated pouch, filled with an electrolyte, and then sealed.

2. Causes of lithium-ion secondary battery failure

Lithium-ion secondary batteries have been on the market for nearly 30 years, but problems of heat generation and ignition still occur to this day. Since the electrolyte in lithium-ion secondary batteries contains flammable organic solvents, abnormal heat generation could easily vaporize these solvents and increase the internal pressure of the batteries, leading to battery rupture and ignition in many cases.

One of the causes of ignition is abnormal heat generation in the batteries due to Joule heat generated by a large current caused by a short circuit between the cathode and anode. There are various causes of short circuit fault, including cases where impurities such as metal powder are mixed into the battery during the manufacturing process, or where the electrodes are deformed by external impact and penetrate the separator. Even in the absence of such physical abnormalities, lithium ions may be reduced and deposited on the anode side due to charge-discharge at a high current, use in low-temperature environments, a low AC ratio, or battery degradation, forming lithium dendrites and short-circuiting the cathode and anode.

These lithium dendrites grow from the anode side and eventually penetrate the separator, causing a short circuit when contact is made with the cathode. As mentioned above, it is considered that in many cases, the separator insulating the cathode and anode loses its function for some reason, resulting in a large short circuit, which leads to abnormal heat generation in the battery. Therefore, the separator plays a very important role in contributing to battery safety.

Lithium-ion secondary battery separators

1. Role and function of separators

The functions of separators required in lithium-ion batteries are insulation of cathode and anode and permeability of lithium ions. Since the basic technology for lithium-ion batteries was established, porous polyolefin (polypropylene or polyethylene) membranes produced by stretching have been mainly used as separators. The porous membranes are insulators and have a dense pore structure, making them suitable for use as separators.

Separators made of polyolefin resin generally melt at temperatures of 130 °C or higher, causing the pores to close (shutdown). When thermal runaway of the battery occurs, the polyolefin melts and becomes non-porous, blocking the movement of lithium ions and stopping the battery from functioning. This shutdown function is one of the basic safety mechanisms of lithium-ion batteries. However, at even higher temperatures, the polyolefin base film will either melt down completely (meltdown) or shrink to the point where it cannot retain its original dimensions, which would cause a short circuit between the cathode and anode.

In order to solve such problems, heat-resistant separators such as ACS and CCS have been developed and applied to lithium-ion secondary batteries. These separators have the ability to maintain their shape after shutdown because the aramid resin and other materials applied to the polyolefin base film improve heat resistance.

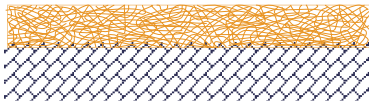
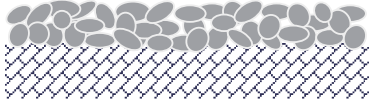
2. Comparison of ACS and CCS

Our ACS is a product obtained by applying a coating solution, which is a mixture of a solvent and aramid resin, to a polyolefin base film. Aramid resins form very

thin, intricately intertwined structures, so the coating layer of ACS on a base film has a very dense pore structure. Since the thermal decomposition temperature of aramid resins is 400 °C or higher, ACS is resistant to thermal contraction and decomposition even in high-temperature environments, and is considered effective in preventing short circuits when the battery generates abnormal amounts of heat. In addition, ACS has a higher void ratio than the base film and has excellent electrolyte retention properties.

On the other hand, CCS is obtained by dispersing ceramics such as alumina together with an aqueous or solvent-based binder and applying the dispersion to a polyolefin base film. In most cases, the ratio of ceramics to binder is 9:1 or less, so the particle size of the ceramics determines the structure of the coating layer. Since solutions containing ceramic particles that are too small in particle size are difficult to coat to base film, relatively large particles (> 0.1 μm) are generally used. This size is large compared to the pore size of polyolefin base film (< 0.1 μm), so the coating layer of CCS has a very coarse structure. Most binders are organic resins such as styrene butadiene rubber (SBR) or polyvinylidene fluoride (PVdF), which have lower thermal decomposition temperatures than aramid resins. Although the heat resistance temperature of the ceramics in CCS is very high, the decomposition temperature of the binder is relatively low, so the coating layer of CCS may rupture when exposed to temperatures of 250 °C or higher. **Table 1** shows the differences between ACS and CCS. Structurally, the ACS coating layer is denser with smaller pore size and has a smoother surface, so it is assumed that lithium ions flow evenly through the coating layer.

Table 1 Comparison of Aramid Coated Separator and Ceramic Coated Separator

	Aramid Coated Separator (ACS)	Ceramic Coated Separator (CCS)
Layer structure		
Heat resistance	High	Low
Materials of coating layer	Aramid (Main component)	Ceramics + Binder (≤several%)
Structure of coating layer	Fine	Coarse

Function of aramid separator (Pervio)

1. Heat resistance

As mentioned above, our ACS is stable up to around 400 °C, and it has been shown to exhibit excellent heat resistance in the temperature range up to that point. The heat resistance of the separator can be confirmed by the heat shape retention ratio at 150 °C. A comparison was made between ACS and CCS designed to the same thickness (base film: 9 μm, coating layer: 3 μm). The shape retention ratio after heating to 150 °C was evaluated by the shape retention change before and after heating, after the separators were cut into squares and placed in an oven at 150 °C for 1 hour. Measurements were taken in the machine direction (MD) and its traverse direction (TD) during separator manufacturing.

Table 2 shows the results; ACS showed over 95% heat shape retention ratio in the MD and TD directions, whereas CCS with the same thickness showed less than 70% retention. Although polyethylene base film shrinks when exposed to high temperatures, the ACS coating layer is presumed to have the ability to withstand the shrinkage of the base film. On the other hand, it is considered that the coating layer of CCS cannot withstand the shrinkage stress, and the entire separator shrinks. The performance for heat shape retention of CCS can be improved by increasing the coating amount, but a disadvantage is that this increases the thickness. As mentioned above, our ACS is a separator that can combine thinness and heat resistance.

2. Lithium dendrite suppression effect

One of the major features of ACS is the heat resistance described above, and another is the structure of its dense coating layer. This feature is assumed to have the effect of uniformly supplying lithium ions during charge-discharge, thereby ensuring uniform reaction distribution on the electrode surface. Since the uniformity and heterogeneity of the reaction may affect the formation of lithium dendrites that cause battery failure, the following studies were investigated.

Table 2 Shape retention ratio of ACS and CCS after 150 °C, 1 h

ACS		CCS	
MD	TD	MD	TD
95% <	95% <	70%	30%

(1) Metallic lithium dendrite deposition behavior on highly oriented pyrolytic graphite (HOPG)

First, the behavior of lithium dendrite formation was evaluated using graphite, a common anode material. As shown in **Fig. 1**, graphite has a layered structure and absorbs lithium ions between the layers, and a more detailed structure is shown in **Fig. 3**.

The hexagonal net planes of graphite are called basal planes, and the edges of the layer formed by overlapping basal planes are called edge planes. When charging starts, lithium ions are inserted between the layers of the graphite anode from the edge planes, but when fully charged, no more lithium ions can enter between the graphite layers. When the potential of the anode is set below 0 V in a fully charged state, lithium ions receive electrons and are deposited as metal. However, it is not known whether the deposition of metallic lithium occurs from the basal planes or edge planes of the graphite.

An electrochemical cell with the configuration shown in **Fig. 4** was used for the evaluation, and HOPG was used for the working electrode (W.E.). HOPG is a highly oriented and pure graphite, and is a commonly used material for modeling evaluations. Metallic lithium was used as the counter electrode (C.E.) and reference electrode (R.E.). For the electrolyte, 1 M LiClO₄ ethylene carbonate (EC)/diethyl carbonate (DEC) (1/1 = vol/vol) was used. Since the purpose of this study is to confirm the lithium dendrite deposition behavior on graphite, no separator was used. The cell was assembled in an argon glove box with a dew point of -70 °C.

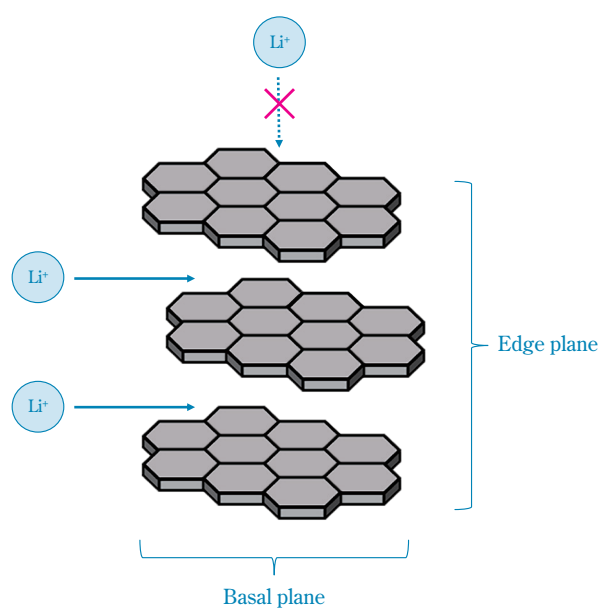


Fig. 3 Structure of graphite and lithium intercalation

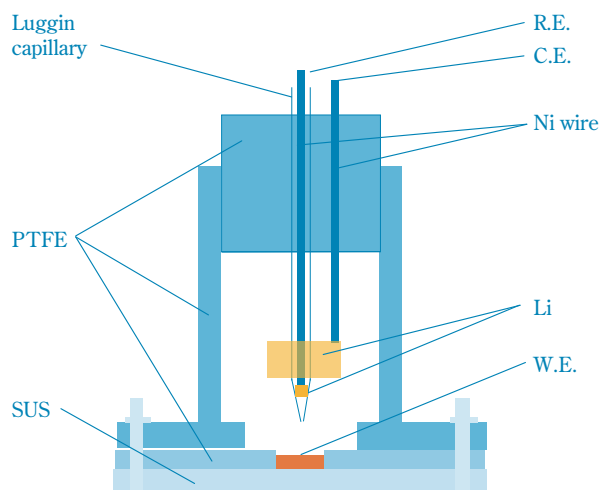


Fig. 4 Schematic diagram of three-electrode electrochemical cell

In the first cycle, the cell voltage was swept from 3 V to 0.005 V at a rate of 0.1 mV/s to form a solid electrolyte interphase (SEI). In the second cycle, the voltage was swept down to 0.005 V at a rate of 0.1 mV/s and held at a constant voltage of 0.005 V for 8 days to reach full charge. Subsequent charging to less than 0 V (-0.01 V, electric quantity 0.05 C) resulted in the deposition of metallic lithium. After the graphite electrode was removed from the cell, the sample was moved in an inert cell filled with argon and observed by SEM under vacuum. The results are shown in Fig. 5.

Fig. 5(a) shows the edge plane and the nearby basal plane, and Fig. 5(b) shows the basal plane (the area away from the edge plane). Comparing Figs. 5(a) and 5(b), it can be seen that an amount of lithium deposits in Fig. 5(a) is larger than in Fig. 5(b). From this result, it was assumed that lithium deposition preferentially

occurs from the edge plane of HOPG.

On the other hand, it was found that lithium deposition also occurs on the basal plane near the edge plane in Fig. 5(a). From the above, it was found that the ease of lithium deposition on graphite is edge plane > basal plane near the edge plane > basal plane. This result is also consistent with the first-principles calculation by Kobayashi *et al.*⁶⁾. To further investigate the morphology of lithium deposition on graphite, it would be important to experimentally measure the reaction ratio between the edge and basal planes.

(2) Measurement of the reaction ratio between edge and basal planes

Quantifying the edge planes of graphite is generally difficult⁷⁾. From the viewpoint that the number of graphite edge planes corresponds to the number of reaction sites, Yamada *et al.* assumed that the number of ions adsorbed on the graphite surface correlates with the number of reaction sites and measured the electric double layer capacitance⁸⁾.

Artificial graphite (MCMB), natural graphite (SNO), and carbon-coated natural graphite were used for evaluation. Those graphite materials and PVdF were mixed in a 9:1 ratio and applied to a copper foil with a doctor blade to make an electrode (60 μm thickness, 5 mg/cm² (graphite equivalent)).

The evaluation was performed on 2032-type coin cells with two graphite electrodes of the same size and thickness. In order to eliminate the influence of the separator as much as possible, CCS with large voids between alumina particles was used as the separator. After assembly, the batteries were left for 12 hours, charged and

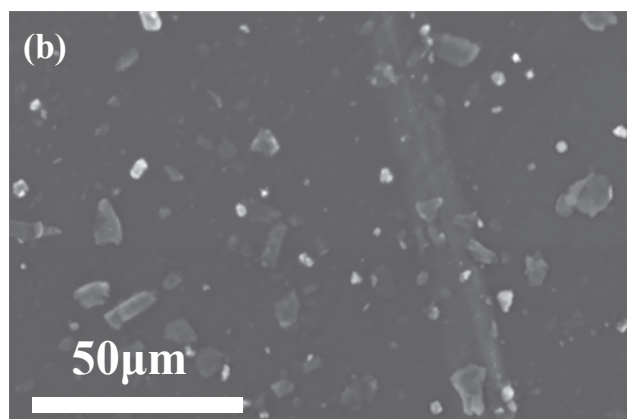
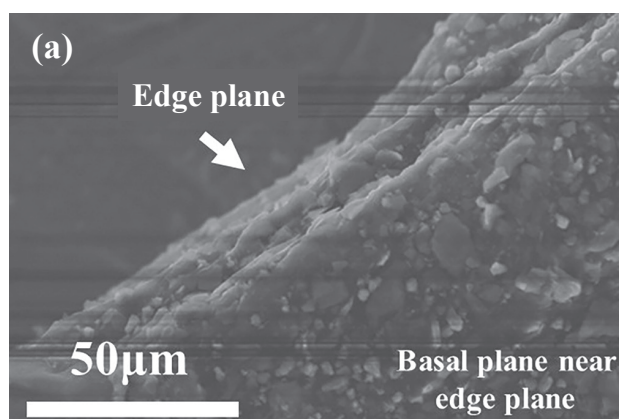


Fig. 5 SEM images of lithium deposition on (a) the edge plane and (b) basal plane surfaces of HOPG

© The Electrochemical Society, Inc. 2022. All rights reserved. Except as provided under U.S. copyright law, this work may not be reproduced, resold, distributed, or modified without the express permission of The Electrochemical Society (ECS). The archival version of this work was published in J. Electrochem. Soc., 169, 010536 (2022).

discharged with a current density of $30 \mu\text{A}/\text{cm}^2$ and a voltage range of 0 to 0.4 V. Their capacitance was calculated using the following formula:

$$C = I \times t / (w \times \Delta V)$$

C : electric double layer capacitance (F/g), I : current (A), t : time (s), w : graphite weight (g), ΔV : the potential difference during charge-discharge processes.

In order to determine the relative amount of edge planes, initial charge-discharge efficiency and double layer capacitance were evaluated. The initial charge-discharge efficiency is correlated with the electric quantity reacted by the electrolyte and graphite electrode, and is also considered to be correlated with the double layer capacitance, because this reaction occurs especially near the edge plane. However, it should be noted that both initial charge-discharge efficiency and double layer capacitance do not represent absolute numbers of edge planes, but rather relative values correlated with edge planes.

Fig. 6(a) shows the relationship between the initial charge-discharge efficiency and the double layer capacitance of the graphite composite electrode. It is considered that the lower the charge-discharge efficiency, the more the electrolyte is decomposed near the edge planes, and the higher the capacitance, the more lithium ions are adsorbed. These correlations suggest that the capacitance is a parameter that correlates with the number of edges on the graphite surface. From the

above, the order of the number of edge planes was found to be natural graphite (SNO-15) > carbon-coated natural graphite > artificial graphite (MCMB). In order to further verify whether the number of edges correlates with the morphology of lithium dendrites, coin cells using Li and graphite as electrodes were assembled and lithium dendrites were deposited on each graphite electrode surface for SEM observation. As shown in Figs. 6(b) to 6(d), lithium dendrites were observed to be deposited in fibrous form on natural graphite, which is considered to have the largest number of edge planes, in granular form on carbon-coated natural graphite, and sparsely in granular form on MCMB. This result suggests that the greater the number of edge planes, the more likely lithium dendrites are deposited in a fibrous form. From the above, it was found that the lithium deposition morphology changes depending on the number of graphite edge planes.

(3) Lithium dendrite deposition on graphite electrodes

Next, in order to conduct the study with an anode material corresponding to that of a commonly widespread battery, the deposition behavior of metallic lithium was confirmed using an electrode made of carbon-coated natural graphite instead of HOPG. In this evaluation, ACS and CCS were used to identify differences between separators.

Lithium deposited in 2032-type coin cells, which were left for 4 hours after assembly and charged at a current density of $0.1 \text{ mA}/\text{cm}^2$ until the voltage went

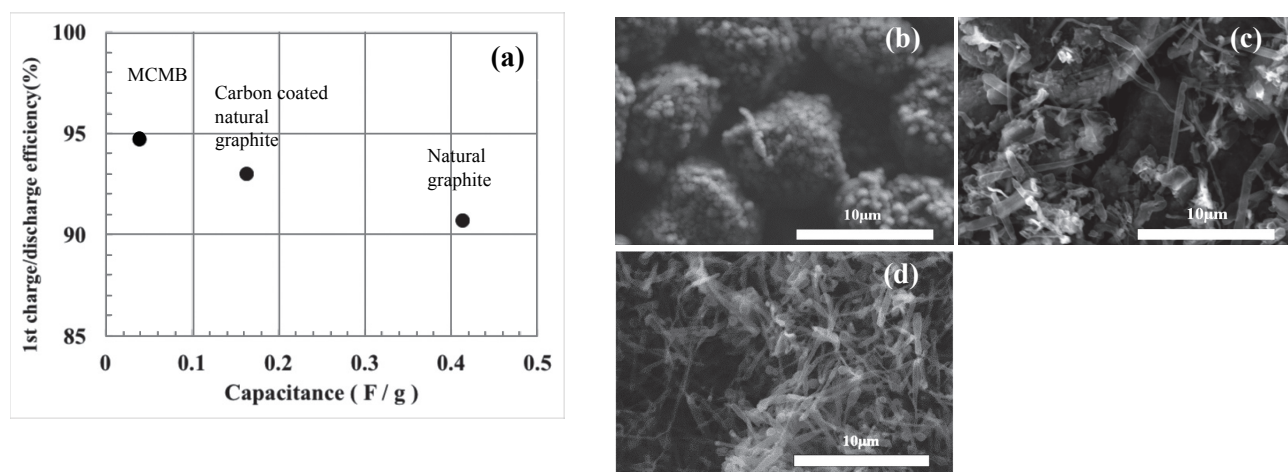


Fig. 6 (a) Relationship between 1st cycle charge-discharge efficiency and the capacitance of different types of graphite. SEM images of lithium deposited graphite, namely, (b) MCMB, (c) carbon coated natural graphite and (d) natural graphite.

© The Electrochemical Society, Inc. 2022. All rights reserved. Except as provided under U.S. copyright law, this work may not be reproduced, resold, distributed, or modified without the express permission of The Electrochemical Society (ECS). The archival version of this work was published in J. Electrochem. Soc., 169, 010536 (2022).

from approximately 3 V to 0.005 V in the first cycle, and again at 0.2 mA/cm² to 0.005 V in the second cycle. The coin cells were then overcharged at 6 mA/cm² for 125 s (electric quantity: 1.5 C) and 333 s (electric quantity: 4.0 C) to deposit lithium dendrites on the graphite electrodes. **Fig. 7** shows the charge-discharge curve for this overcharge. SEM observations were made under vacuum at point A (electric quantity: 1.5 C) and point B (electric quantity: 4.0 C).

Figs. 8(a) and **8(b)** are SEM images at point A in **Fig. 7**. **Fig. 8(a)** shows the results when ACS was used as the separator, where most of the lithium dendrites deposited in granular. In contrast, as shown in **Fig. 8(b)**, lithium dendrites were deposited in the form of elongated fibers when CCS was used. **Figs. 8(c)** and **8(d)** are SEM images at point B in **Fig. 7**. The reacted electric quantity was greater at point B than at point A. The amount of deposits increased at point B. The increase

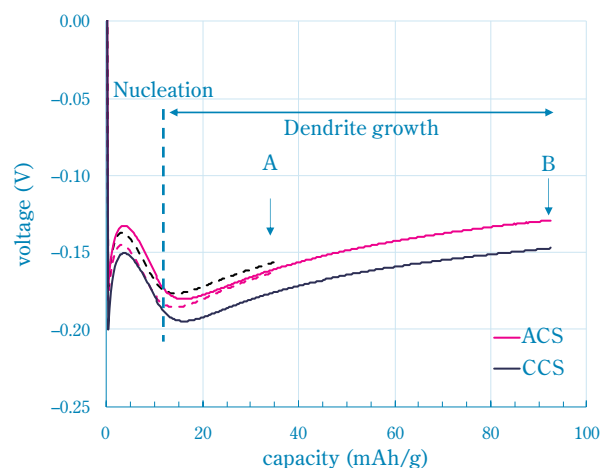


Fig. 7 Example of a charging curve with lithium deposition. Points A and B are SEM observation points. The weight represented on the x-axis is that of graphite. The x-axis represents overcharge capacity. Created using data from cited reference 9).

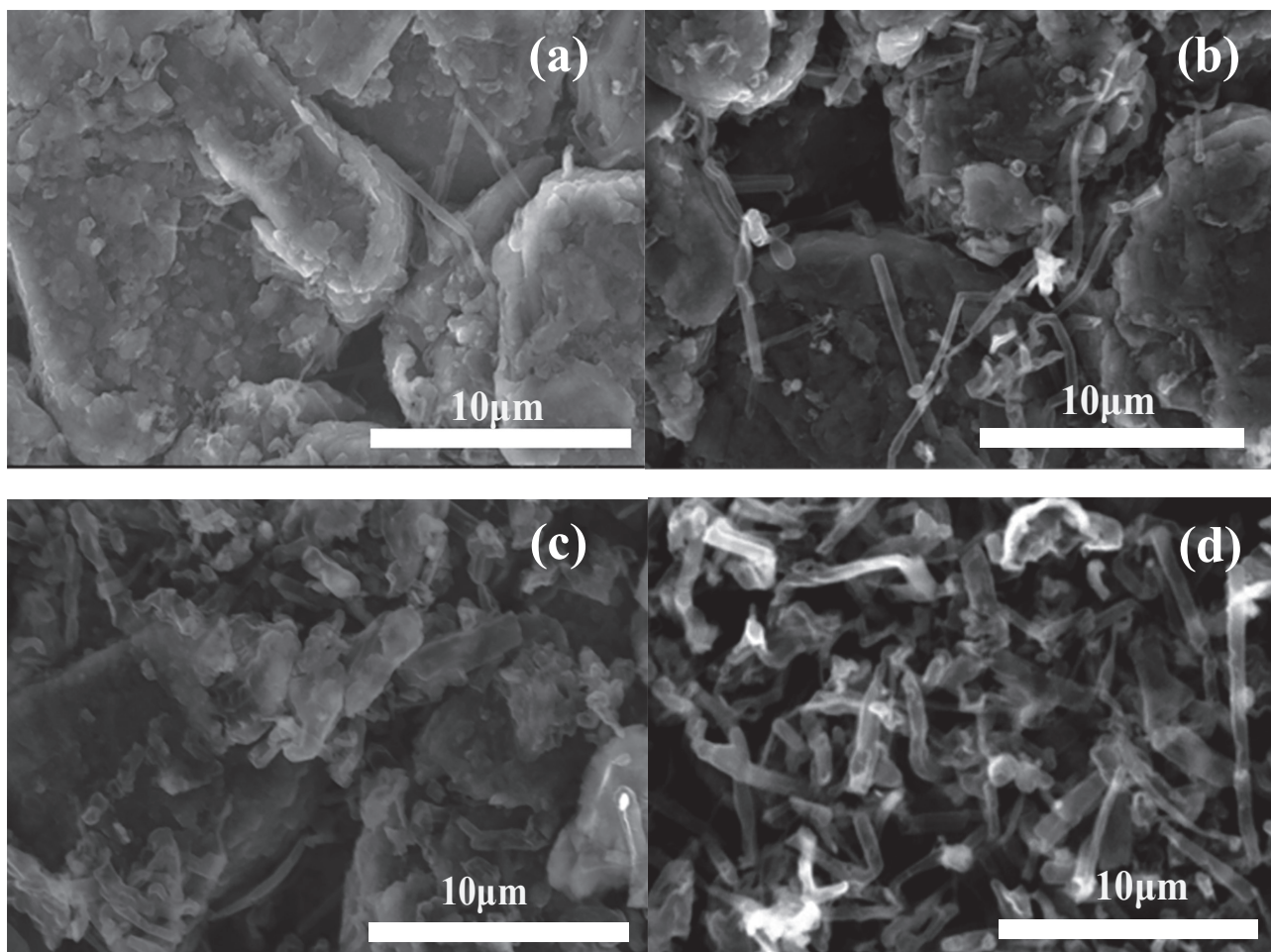


Fig. 8 SEM images of 1.5 coulombs of lithium deposited through the (a) ACS and (b) CCS and 4 coulombs of lithium deposited through the (c) ACS and (d) CCS

© The Electrochemical Society, Inc. 2022. All rights reserved. Except as provided under U.S. copyright law, this work may not be reproduced, resold, distributed, or modified without the express permission of The Electrochemical Society (ECS). The archival version of this work was published in *J. Electrochem. Soc.*, 169, 010536 (2022).

in deposits was especially significant when CCS was used as shown in Fig. 8(d), where a large amount of fibrous lithium dendrites were generated. In comparison, no significant generation of fibrous lithium dendrites was observed when ACS was used, as shown in Fig. 8(c). Fig. 9 shows the growth behavior of lithium dendrites confirmed by overcharging at a current density of 1 mA/cm² for 84 seconds (electric quantity: 1.0 C).

Figs. 9(a) and 9(b) show the results when ACS was used as the separator. In Fig. 9(a), it was confirmed that the tips of the generated fibrous lithium dendrites contacted the ACS while growing and were deformed into granular. In Fig. 9(b), the generated lithium dendrites grew and deformed laterally as if they were crushed on the surface of the ACS. These indicate that the growing lithium dendrites may have buckled due to the smoothness and stiffness of the aramid resin surface when they came into contact with the ACS.

On the other hand, when CCS was used, as shown in Fig. 9(c), the lithium dendrites generated were less particulate and maintained a fibrous form, and were longer (larger aspect ratio) than those generated when using ACS. If the lithium dendrites grow fibrous and the deposition reaction continues, they may break through the separator and cause a short circuit, which is dangerous. In addition, the relationship between the reacted electric quantity and the aspect ratio of the

lithium dendrites was generated using an image analysis software (ImageJ). The aspect ratio was determined by the ratio of the lengths of the long and short sides, as shown in Fig. 9(d). Figs. 9(e) and 9(f) show the aspect ratios of lithium dendrites generated on the graphite anode when ACS and CCS were used, respectively. In both cases, as the reacted electric quantity increased, the frequency of contact with the separator surface increased and the lithium dendrites bent, which is thought to have caused the aspect ratio to behave in a decreasing manner.

The aspect ratios were in the order ACS < CCS, which may be attributed to the pore structure of the separator. It is assumed that the small pores of ACS make it difficult for lithium dendrites to penetrate into the internal pores even if they come into contact with the aramid surface. When compared with the same reacted electric quantity, it is assumed that the large voids in the coating layer of CCS make it easier for the generated lithium dendrites to grow inside the voids of the coating layer while maintaining their fibrous form. These phenomena and analytical results suggest that ACS has a superior function to CCS with respect to lithium dendrite growth suppression.

(4) Observation of lithium dendrite deposition

As mentioned above, it was found that lithium dendrites

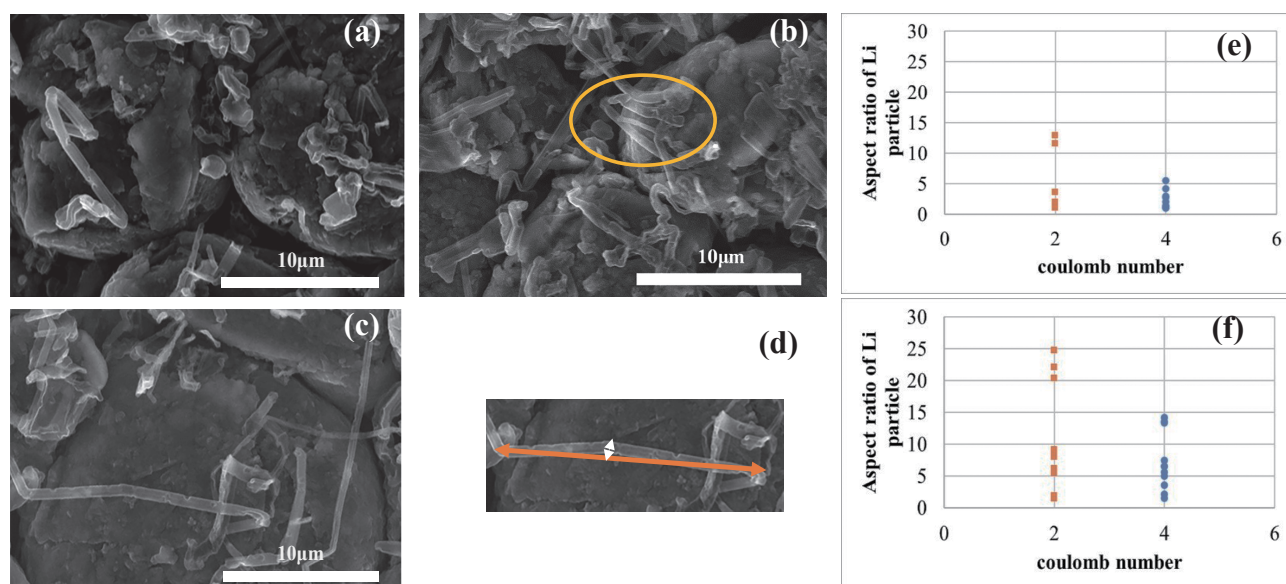


Fig. 9 SEM images of (a) when ACS was used, partially bent dendrites; (b) when ACS was used, dendrites were squashed; (c) when CCS was used, the dendrites remained fibrous and became long. (d) Example of the aspect ratio of a dendrite. Aspect ratios of dendrites on graphite when (e) ACS and (f) CCS were used.

© The Electrochemical Society, Inc. 2022. All rights reserved. Except as provided under U.S. copyright law, this work may not be reproduced, resold, distributed, or modified without the express permission of The Electrochemical Society (ECS). The archival version of this work was published in J. Electrochem. Soc., 169, 010536 (2022).

were generated differently when ACS was used compared to when CCS was used. In order to observe the situation in detail, the electrode surface condition after lithium dendrite deposition was also evaluated. The evaluation cell is the same as in Fig. 4, but a copper foil was used for the working electrode, and a separator was placed so that the coating layer was in contact with the copper foil. After the first cycle, lithium dendrites were deposited on the copper foil by charging at a current density of 1 mA/cm^2 for 16.5 minutes. The cells were then disassembled in an argon glove box, and the inert cells were used for image observation by optical microscopy and evaluation by surface roughness meter.

Figs. 10(a) and 10(b) show optical microscope images of the systems with ACS and CCS, respectively. In both cases, the fibrous tips were in contact with each other, but most of the lithium dendrites in the system

with CCS maintained their fibrous shape. Figs. 10(c) and 10(d) show the results of surface roughness measurements, which indicate that lithium dendrites deposited through ACS form a smooth surface, while those deposited through CCS form a large uneven surface. Since more uniform deposition occurred in the system with ACS, it is assumed that the deposition reaction on the electrode occurred uniformly, which is a reasonable result considering the uniformity of the aramid resin pores.

(5) Effects in cycle test

Furthermore, the effect of lithium dendrite formation behavior on the cycle characteristics of the battery was investigated. The effect was evaluated by repeated dissolution and deposition of lithium dendrites on copper foil (pulse cycle test). For evaluation, 2032-type coin

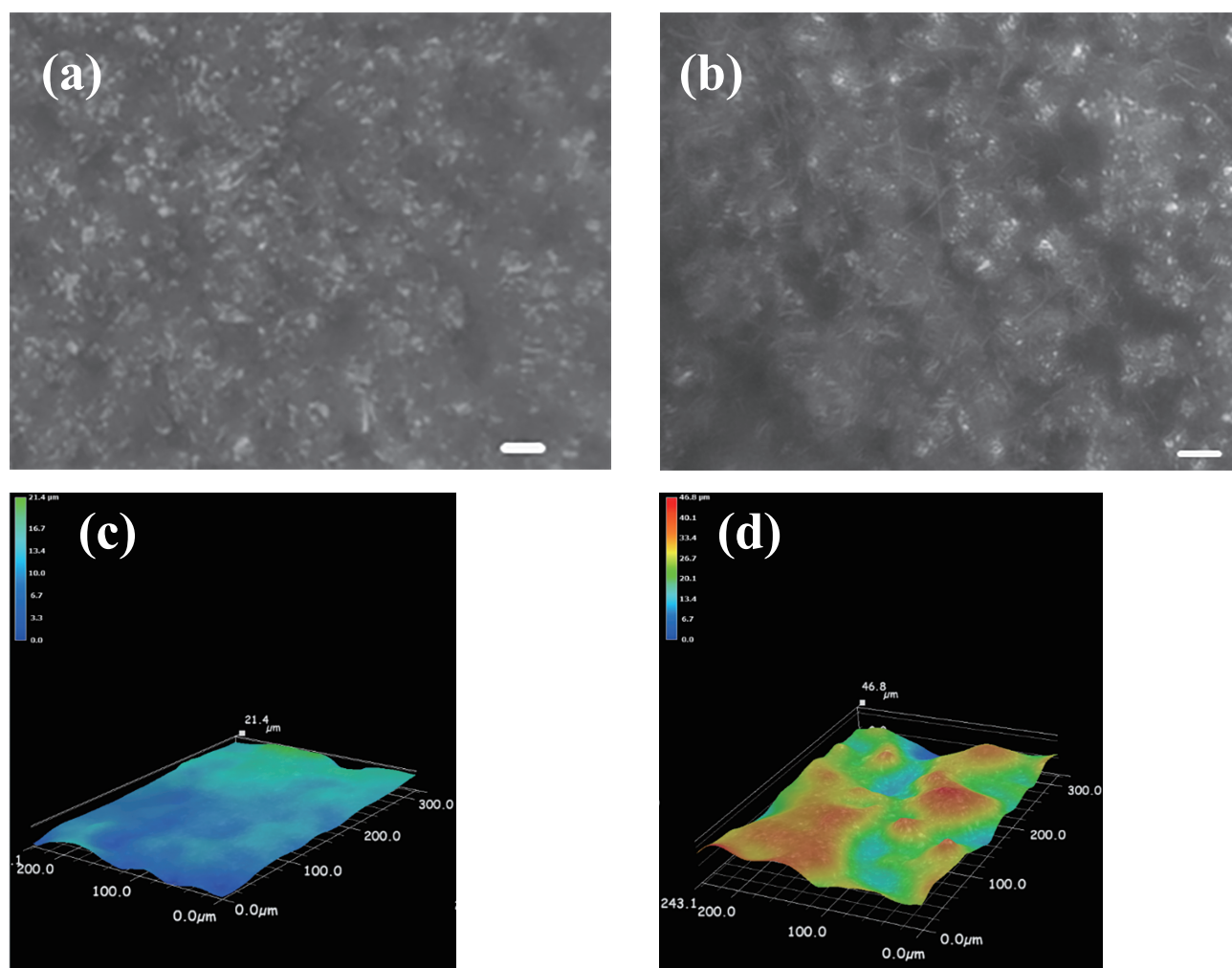


Fig. 10 Optical microscope images of dendrite deposition at a current density of 1 mA/cm^2 for 16.5 min through (a) ACS and (b) CCS. Focus stacked images for when (c) ACS and (d) CCS were used.

© The Electrochemical Society, Inc. 2022. All rights reserved. Except as provided under U.S. copyright law, this work may not be reproduced, resold, distributed, or modified without the express permission of The Electrochemical Society (ECS). The archival version of this work was published in J. Electrochem. Soc., 169, 020546 (2022).

cells were used with copper and metallic lithium foil as electrodes and ACS and CCS as separators. The coin cells were left for 4 hours after assembly, charged at a current density of 1 mA/cm^2 for 5,000 seconds to deposit lithium, and then tested at a current density of 2 mA/cm^2 , a cutoff voltage of $\pm 0.5 \text{ V}$, and a pulse width of 250 seconds.

Fig. 11 shows the results of the pulse cycle test. The time to reach the cutoff voltage ($\pm 0.5 \text{ V}$) for the dissolution-deposition reaction was 7.1 hours for ACS and 6 hours for CCS, indicating that the cutoff voltage was

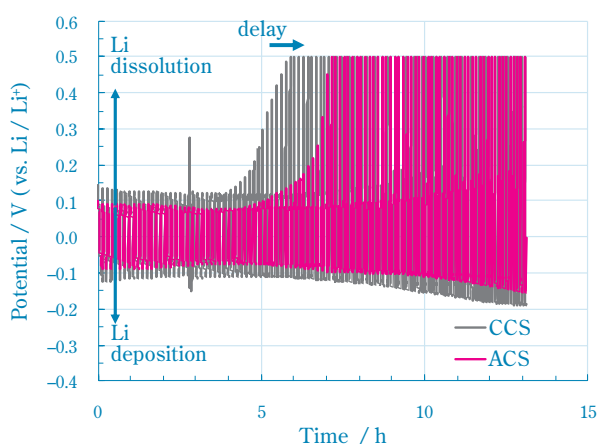


Fig. 11 The voltage behavior during pulse cycling with each separator
Created using data from cited reference 9).

reached earlier for CCS. In this pulse cycle test, lithium dendrites are repeatedly dissolved and deposited. However, some of the deposited lithium dendrites cannot maintain conduction and become lithium that does not contribute to the reaction (dead lithium), causing resistance to rise and capacitance to drop. Since the CCS coating layer has large voids, fibrous metallic lithium is likely to generate between the voids. Lithium dendrites generated in fibrous form may be prone to break off and become dead lithium because they react from the root. With ACS, lithium dendrites form in granular, so the tips are less likely to break off and dead lithium is less likely to form. Therefore, it is assumed that the smooth dissolution and deposition during charging and discharging improved the results of the pulse cycle test. Such functions are also effective for a graphite anode, and may also be effective when metallic lithium is used for the anode.

Function of aramid separator in lithium dendrite suppression

This study revealed that ACS has a different lithium dendrite deposition morphology compared to CCS. This feature is thought to be derived from the structure of the coating layer, and the presumed mechanism is shown in Fig. 12.

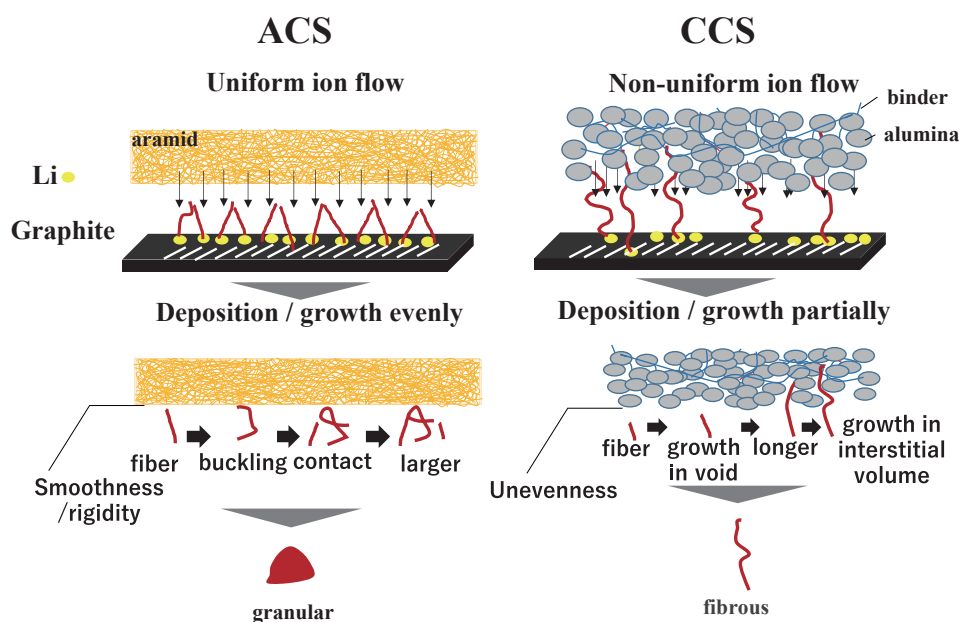


Fig. 12 Schematic diagram of estimated lithium dendrite deposition mechanism through ACS and CCS
© The Electrochemical Society, Inc. 2022. All rights reserved. Except as provided under U.S. copyright law, this work may not be reproduced, resold, distributed, or modified without the express permission of The Electrochemical Society (ECS). The archival version of this work was published in J. Electrochem. Soc., 169, 010536 (2022).

Since the ACS coating layer has a very dense and uniform structure, it is assumed that lithium ions pass through the ACS uniformly and the smooth lithium dendrite deposition reaction occurs uniformly. Even when lithium dendrites grew, they could not pass through the dense, smooth aramid layer and were likely folded to form granular lithium dendrites on the graphite. On the other hand, the CCS coating layer has a very rough structure and non-uniform ion flow, which is thought to cause localized reactions. In addition to this, the large voids in the coating layer are assumed to cause the growth of lithium dendrites inside the coating layer as well.

The problem of lithium dendrites is that they cause short-circuits between the cathode and anode. Therefore, it is presumed that ACS, which can suppress lithium dendrite growth by forming granular, performs better in terms of short-circuit prevention compared to CCS, which can easily grow lithium dendrites in fibrous form in the thickness direction of the separator.

Acknowledgments

We would like to express our sincere gratitude to the members of the Abe Laboratory and the professors of the Department of Energy and Hydrocarbon Chemistry for their generous support in this research.

Reference

- 1) M. Armand *et al.*, J. Power Sources, 479, 228708 (2020).
- 2) J. Jang *et al.*, Materials, 13, 4625 (2020).
- 3) Y. Xiang *et al.*, ChemSusChem, 9, 3023 (2016).
- 4) H. Lee *et al.*, Energy Environ. Sci., 7, 3857 (2014).
- 5) P. V. Chombo and Y. Laonual, J. Power Sources, 478, 228649 (2020).
- 6) K. Kobayashi, Phys. Rev. B 48, 1757 (1993).
- 7) T. Ishii *et al.*, Carbon, 125, 146 (2017).
- 8) Y. Yamada *et al.*, Langmuir, 26(18), 1499 (2010).
- 9) I. Arise *et al.*, J. Electrochem. Soc., 169, 010536 (2022).

PROFILE



Ichiro ARISE

Sumitomo Chemical Co., Ltd.
Energy & Functional Materials Research Laboratory
Research Associate, Ph.D.
(Current department: IT-Related Chemicals
Research Laboratory)



Kohei MIYAZAKI

Kyoto University
Department of Energy and Hydrocarbon
Chemistry
Associate Professor, Ph.D.



Tomoaki OZEKI

Sumitomo Chemical Co., Ltd.
Energy & Functional Materials Research
Laboratory
Research Associate



Takeshi ABE

Kyoto University
Department of Energy and Hydrocarbon
Chemistry
Professor, Ph.D.



Yuto MIYAHARA

Kyoto University
Department of Energy and Hydrocarbon
Chemistry
Assistant Professor, Ph.D.